Energy Storage Materials 41 (2021) 203–208

Contents lists available at ScienceDirect

Energy Storage Materials

journal homepage: www.elsevier.com/locate/ensm

Enhanced supercapacitive performance of $Mo_{1.33}C$ MXene based asymmetric supercapacitors in lithium chloride electrolyte

Ahmed El Ghazaly[a], Wei Zheng[a], Joseph Halim[a], Eric Néstor Tseng[b], Per OÅ Persson[b], Bilal Ahmed[a,*], Johanna Rosen[a,*]

[a] Materials Design Division, Department of Physics, Chemistry and Biology (IFM), Linköping University, 581 83 Linköping, Sweden
[b] Thin Film Physics Division, Department of Physics, Chemistry and Biology (IFM), Linköping University, 581 83 Linköping, Sweden

ARTICLE INFO

Keywords:
$Mo_{1.33}C$
MXene
Asymmetric supercapacitors, LiCl electrolyte

ABSTRACT

Two-dimensional (2D) $Mo_{1.33}C$ MXene renders great potential for energy storage applications and is mainly studied in the sulfuric acid (H_2SO_4) electrolyte. However, H_2SO_4 limits the electrode potential to 0.9 V for symmetric devices and 1.3 V for asymmetric devices. Herein, we explore the electrochemical behavior of $Mo_{1.33}C$ MXene in LiCl electrolyte. In comparison to H_2SO_4, LiCl electrolyte is a neutral salt with high solubility at room temperature and low hazardousness. The analysis shows a volumetric capacitance of 815 Fcm^{-3} at a scan rate of 2 mVs^{-1} with a large operating potential window of -1.2 to +0.3V (*vs.* Ag/AgCl). This is further exploited to construct MXene-based asymmetric supercapacitors $Mo_{1.33}C//Mn_xO_n$, and the electrochemical performance is evaluated in 5M LiCl electrolyte. Owing to the wide voltage widow of the $Mo_{1.33}C//Mn_xO_n$ devices (2V) and high packing density of the electrodes, we have achieved a volumetric energy density of 58 mWh/cm^3, a maximum power density of 31 Wcm^{-3} and retained 92% of the initial capacitance after 10,000 charge/discharge cycles at 10 A g^{-1}. One of the main value propositions of this work, aside from the high energy density, is the outstanding columbic efficiency (100%), which ensures excellent cyclic stability and is highly desirable for practical applications.

Introduction

The high-power output, aside from the low environmental impact and safety, makes aqueous electrolyte supercapacitors (SCs) one of the most promising energy storage devices [1]. In general, SCs are operated using aqueous electrolytes, resulting in a smaller voltage window (≈1.2 V), while the SCs based on organic and ionic electrolytes exhibit a higher voltage window (≈3-4 V), leading to a high energy density [2]. Extending the potential window decomposes the aqueous electrolyte at the electrode/electrolyte interface and leads to undesirable side reactions, material degradation and performance deterioration. On the other hand, the utilization of ionic or organic electrolytes raises handling, safety, and cost concerns. Therefore, it is highly motivated to extend the operating voltage window of SCs with aqueous electrolytes.

The discovery of two-dimensional (2D) Ti_3C_2 MXene with a volumetric capacitance of 900 Fcm^{-3}, reaching further up to 1500 Fcm^{-3} after a hydrogel treatment process [3], a high conductivity (20,000 Scm^{-1}), and high capacitance retention, has extended the chances of developing MXene-based commercialized energy storage devices [4-6]. Another member of the MXene family, *i.e.,* $Mo_{1.33}C$ *i*-MXene, has delivered a far higher volumetric capacitance of 1150 Fcm^{-3} due to the presence of ordered vacancies, originating from the selective removal of both Sc and Al from the parent $Mo_{2/3}Sc_{1/3}AlC$ *i*-MAX phase [7-9]. Moreover, the thermal treatment and mixing of $Mo_{1.33}C$ with PEDOT: PSS, cellulose or biopolymers have further improved the specific capacitance, cyclic stability, and rate performance [7,10-12]. However, these studies are carried out using H_2SO_4 electrolyte, where $Mo_{1.33}C$ exhibits a pseudocapacitive charge storage mechanism with an obvious couple of redox peaks. It worth emphasizing that the redox reactions occurring in the acidic electrolyte due to the variation in transition metal oxidation states, aside from the hydronium ion intercalation, is the main contributor to the increased capacitance [8,11].

Also, it has been observed that the voltage window of $Mo_{1.33}C$ MXene with stainless-steel, as a current collector, is limited to 0.65 V. However, the operating voltage window can be extended towards the negative side by using glassy carbon (GC) as a current collector, which suppresses the hydrogen evolution reaction (HER) and results in a voltage window of 0.8 V. The positive potential side for MXene electrodes is always limited by the open-circuit voltage (OCV) to avoid undesirable phase transformations and/or MXene oxidation [5].

* Corresponding authors.
E-mail addresses: Bilal.Ahmed@liu.se (B. Ahmed), Johanna.Rosen@liu.se (J. Rosen).

https://doi.org/10.1016/j.ensm.2021.05.006
Received 26 February 2021; Received in revised form 26 April 2021; Accepted 5 May 2021
Available online 14 May 2021

Previous studies have proven that widening the voltage widow of MXene can be achieved by improving the redox reaction dynamics [13] *via* (*i*) changing the electrolyte pH, (*ii*) using multi-ion electrolytes, such as redox-active electrolyte [14], or (*iii*) dissolving an excessive amount of salt in water, such as a high molarity lithium chloride (LiCl) [15]. The latter can potentially extend beyond the thermodynamics potential [16]. For instance, V_2C and Ti_3C_2 have demonstrated an operating potential window of 0.9 V and 1.3 V (*vs.* Ag/AgCl) in 5M LiCl, respectively [17]. MXene-based symmetric SCs are limited to the operating voltage of 1 V in basic electrolytes due to the low oxidation potential of MXene. Therefore, high-performance MXene-based devices can be constructed by combining MXene as a negative electrode with a high-performance positive electrode, forming asymmetric SCs. Many efforts have been devoted to introduce a suitable positive electrode to match the superior charge storage performance of MXene-based negative electrodes, such as carbon-based electrodes [18], conducting polymers [19] and metal oxides [20]. However, the energy density of these MXene-based ASCs is either limited by the operating potential or the specific capacitance of the positive electrode.

Manganese oxide is a promising electrode material because of multiple oxidation states of the transition metal (from +2 to+ 7) [21], wide operating potential and high capacitance [21]. However, the electrochemical stability of MnO_2 in aqueous electrolytes is compromised due to the change in physiochemical properties and the capacitance of MnO_2 electrode fades during the charge/discharge cycling [22]. Still, Mn_3O_4 electrode renders a high theoretical capacitance of 1400 Fg^{-1} and outstanding stability in aqueous electrolyte [23,24].

Motivated by the above, the current study investigates the electrochemical behavior of $Mo_{1.33}C$ MXene in 5M LiCl electrolyte and exploits the wide voltage window (1.5 V) of $Mo_{1.33}C$ electrode to construct asymmetric supercapacitors (MXene//Mn_xO_n), where Mn_xO_n served as a positive electrode. The high voltage window yielded the volumetric and gravimetric capacitance of ~815 Fcm^{-3} and 215 Fg^{-1}, respectively, at a scan rate of 2 mVs^{-1}. Furthermore, the ASC (MXene//Mn_xO_n) demonstrated a maximum energy density of 58 mW h/cm^3 at 1 Ag^{-1}, high stability (92%) and excellent Coulombic efficiency (100%) at 10 Ag^{-1}.

2. Experimental methods

MXene synthesis: The $Mo_{2/3}Sc_{1/3}AlC$ *i*-MAX phase precursor was prepared by using Mo (99.9%, Sigma Aldric), Sc (99.99% Stanford Advanced), Al (99.8%, Alfa) and C (99.9%, Sigma Aldric), as detailed elsewhere [8]. To prepare $Mo_{1.33}C$ MXene, 2 g of *i*-MAX phase was added into 20 mL of 50 % hydrofluoric acid (HF) for 24 hrs, followed by successive washing with deionized water till the pH reached 6. Then, the delamination of as-etched powder was achieved by adding 10 mL of 40 wt.% TBAOH ,Afterwards, 40 ml of deionized water were added to the sediment and the mixture was manually shaken for 5 min followed by centrifugation at 3000 rpm for 1h. The supernatant was collected and filtered to obtain a free-standing film. The electrode density of $Mo_{1.33}C$ was 3.75 gcm^{-3}, which is consistent with the previously reported density of $Mo_{1.33}C$ MXene films [8].

Mn_xO_n synthesis: $MnSO_4$ powder (HACH Company, USA) was mixed with NaOH (99.99%, Honeywell, Germany) in a molar ratio of 1:2. The mixture was stirred for 24 hrs and then aged for 1 hr at room temperature. The as-produced powder was mixed with PTFE and carbon black (with a mass ratio of 7:2:1) to form a ~7 μm thick film with a density of ~3 g cm^{-3}.

Materials characterization: The morphology of Mn_xO_n and MXene were observed using a field emission scanning electron microscope (FE-SEM, ZEISS). The XRD patterns were collected using an X-ray diffractometer (Rigaku, prefix), equipped with Cu Kα radiations (λ = 1.54 Å). The step size was 0.02° and the scan rate was 0.5 sec/step. STEM (FEI Titan^3 60-300) was used to investigate $Mo_{1.33}C$ filmin cross section.

Electrochemical characterization: The electrochemical behavior was studied using a Swagelok plastic cell, filled with 5M LiCl electrolyte. The glassy carbon electrodes served as current collectors, activated carbon (containing 5 wt. % PTFE) acted as the counter electrode and Ag/AgCl (3.5M KCl) served as the reference electrode. Thin films of $Mo_{1.33}C$ (~5 μm) and Mn_xO_n (~7 μm) were separately employed as working electrodes. The capacitive performance was investigated by using cyclic voltammetry (CV) at different scan rates (2-500 mV s^{-1}) and galvanostatic charge/discharge at different current densities (1-10 Ag^{-1}). Electrochemical impedance spectroscopy (EIS) was carried out in the frequency range of 100 mHz to 100 kHz. A sinusoidal voltage of 10 mA was applied during EIS. The capacitance was calculated by integrating the discharge area in the CV curves according to $C_g = 1/\Delta V \upsilon E_m$ ($\int$ idv), where *i* represents the discharge current, *V* refers to voltage window, υ corresponds to scan rate and E_m denotes the electrode mass. The capacitive and diffusion contributions can be calculated from the following equation:

$$i(V) = k_1\upsilon + k_2\upsilon^{1/2}$$

where i(V) refers to the current as a function of specific voltage,*v* represents the scan rate, and k_1 and k_2 are constants.

Fabrication of asymmetric supercapacitors: The ASCs were fabricated using $Mo_{1.33}C$ MXene as negative electrodes, Mn_xO_n film as positive electrodes and Celgard 3200 as separators. Total electrodes' mass in the device was ~0.3 mg loaded on 3 mm diameter current collector. The current collector and electrolyte were glass carbon and 5M LiCl, respectively. The electrode weight was calculated according to $(C_1m_1V_1)_{Mo1.33C} = (C_2m_2V_2)_{MnxOn}$. The energy density ($E_g$) and power density (P) were calculated through the following equations:

$$E_g = 0.5\, C_g V^2$$

$$E_v = \rho \times E_g$$

$$P = E_v/t$$

where ρ represents the volumetric density based on the two electrodes volumes and *t* refers to the discharge time. The Mn_xO_n powder mixed with 10 wt.% PTFE and 20 wt.% carbon black was rolled, dried and punched to obtain the discs of desired size. The film thickness was measured using cross-sectional SEM images.

Results and discussion

The synthesis protocol of $Mo_{1.33}C$ MXene and Mn_3O_4/ $Na_{0.55}Mn_2O_4$ mixture (Mn_xO_n) is presented in Fig. 1a. $Mo_{1.33}C$ MXene was first prepared by selective etching of scandium (Sc) and aluminum (Al) from $Mo_{2/3}Sc_{1/3}AlC$ *i*-MAX phase using HF, followed by washing and TBAOH-assisted delamination. Finally, the colloidal suspension was vacuum filtered to obtain free-standing MXene films with an average thickness of 5 μm, see Fig. 1c.The STEM image, Fig. S1, confirms the well-aligned layered structure of single MXene sheets. The Mn_xO_n powder was prepared by mixing NaOH platelets and $MnSO_4$ powder and stirring for 24 h (Fig.1b), resulting in the formation of a cylindrical oxide structure (Fig.1d).

XRD patterns of as-prepared Mn_xO_n powder and $Mo_{1.33}C$ film are presented in Fig. S2. The $Mo_{1.33}C$ showed an obvious (002) MXene peak at a low diffraction angle (5.6°) with no evidence of any residual MAX phase or ScF_3. The diffraction peaks of Mn_xO_n indicate the presence of two different manganous oxide phases, i.e., Mn_3O_4 and $Na_{0.55}Mn_2O_4.1.5H_2O$ (Fig. S3). The high-magnification SEM images in Fig. S3(a-c) reveal that the as-prepared Mn_xO_n powder consists of small, agglomerated nanoparticles and well-delineated nanosheets. The EDS mapping shows uniform distribution of Mn and O, whereas the carbon originates from the carbon black and PTFE, and a small amount of sodium (Na, <1 at. %) originates from $Na_{0.55}Mn_2O_4$ phase (Fig. S3e). The cross-sectional SEM image of the Mn_xO_n film is presented in Fig. S4.

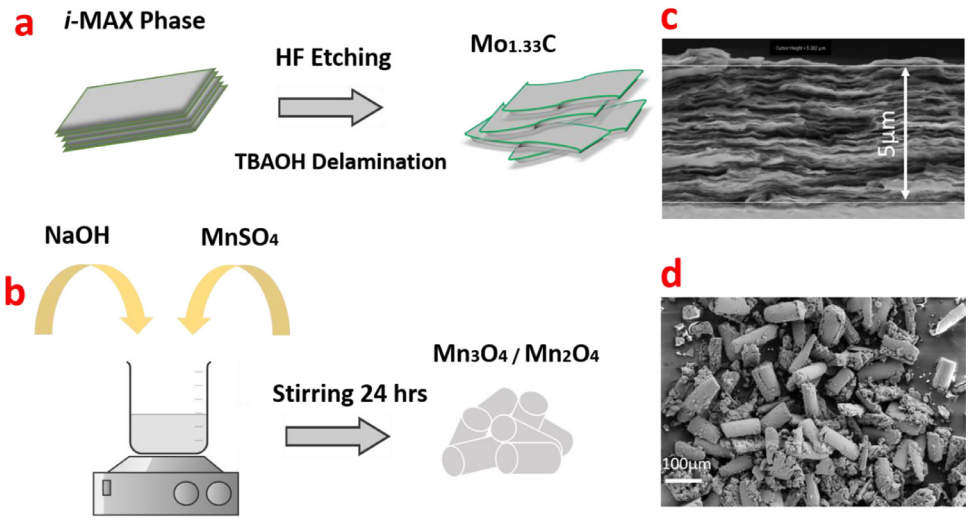

Fig. 1. (a) Schematic illustration of the synthesis of $Mo_{1.33}C$ MXene film; (b) Synthesis procedure of the Mn_xO_n powder; (c) Cross-sectional SEM image of the $Mo_{1.33}C$ MXene film; and (d) Low-magnification SEM image of Mn_xO_n powder.

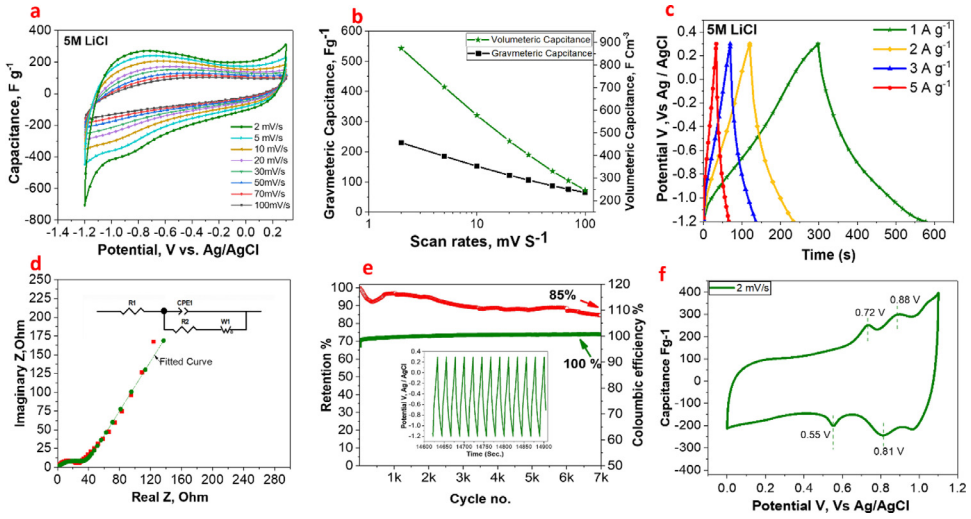

Fig. 2. (a) CV curves of $Mo_{1.33}C$ plotted based on specific capacitances at different scan rates (2-100 mV s^{-1}); b) Gravimetric and volumetric capacitance at different scan rates; c) Galvanostatic charge/discharge curves at different current densities; d) Nyquist plot with the equivalent circuit; e) Cyclic stability and Coulombic efficiency at 10 A g^{-1}; and f) CV curve of Mn_xO_n electrode at 2 mV s^{-1}.

The electrochemical behavior of $Mo_{1.33}C$ MXene in 5M LiCl aqueous electrolyte is demonstrated in Fig. 2. The low and high potential limits were assigned using glassy carbon as a current collector, as shown in Fig. S5. The $Mo_{1.33}C$ voltage window can be extended to +0.3 V and -1.2 V (*vs.* Ag/AgCl) in the positive and the negative directions, respectively. The high concentration of LiCl decreases the amount of free water molecules and, consequently, limits the parasitic reactions at the negative side [2]. The operating potential window of $Mo_{1.33}C$ in 5M LiCl electrolyte (1.5 V) is higher than the previously reported Ti_3C_2 (1.35 V) and V_2C (1V) MXenes under the similar operating conditions. The CV profiles of $Mo_{1.33}C$ MXene, at the scan rate of 2 to 100 mV s^{-1}, exhibit a broad redox peak at -0.9 V (*vs.* Ag/AgCl), which is an indication of the pseudo-intercalated capacitive behavior, as reported for MXenes in aqueous electrolytes (Fig. 2a) [4][17]. Gravimetric and volumetric capacitances of the $Mo_{1.33}C$ electrode at different scan rates are shown in Fig. 2b. The $Mo_{1.33}C$ electrode delivered a volumetric capacitance of 815, 684, 560, 449, 388, 319, 277 and 238 Fcm^{-3} at the scan rate of 2, 5, 10, 20, 30, 50, 70 and 100 mVs^{-1}, respectively. Correspondingly, the gravimetric capacitance was found to be 215, 183, 150, 120, 103, 85, 73 and 63 Fg^{-1} at the same scan rates, respectively.

One should note that the $Mo_{1.33}C$ electrode has higher capacitance than the Ti_3C_2 (130 F g^{-1}) and V_2C (110 F g^{-1}) free-standing MXene films measured in 5M LiCl electrolytes at the same scan rate (2 mV s^{-1}) [17]. In addition to the larger potential window (1.5 V), the high capacitance of $Mo_{1.33}C$ MXene may be ascribed to the presence of vacancies, originating from the removal of Sc during the etching process. As reported in the case of 1M H_2SO_4 electrolyte [8], the vacancies-containing $Mo_{1.33}C$ electrode renders ~65% higher capacitance than the vacancies-free counterpart, i.e., Mo_2C MXene. Insight into whether this capacitance difference is due to the vacancies alone, or the observed difference in the surface terminations, requires further investigations. Still, it has been reported that the presence of vacancies in 2D materials may improve the electrochemical behavior such as for TiS_2 [25]. Also, a theoretical study on Mo_2C reported that the presence of atomic vacancies improves the adsorption and diffusion of Li-ions on Mo_2C surface [26]. Fig. 2c presents GCD curves of the $Mo_{1.33}C$ at the current density of 1, 2, 3 and 5 Ag^{-1}, showing a symmetric triangular shape without obvious IR drop. This also confirms the high reversibility of redox reactions at the $Mo_{1.33}C$ electrode/electrolyte interface. EIS analysis in Fig. 2d represents the experimental and fitted Nyquist plots. TheNyquist plot of $Mo_{1.33}C$ can be fitted with an equivalent circuit, which is similar to Ti_3C_2 electrodes [15,27] because the Nyquist plot behaves like Ti_3C_2 in 5M LiCl [27], containing a semicircle in the high-frequency region and a sloping line in the low-frequency region. The internal resistance (0.9 Ω) and charge transfer resistance (8.3 Ω) can be estimated from the *x*-intercept and semicircle diameter in the high-frequency region, respectively.

$Mo_{1.33}C$ MXene retained >85% of the initial capacitance after 7,000 charge/discharge cycles at the current density of 10 Ag^{-1}, as shown in Fig. 2e. In comparison, a previous report showed that V_2C MXene suf-

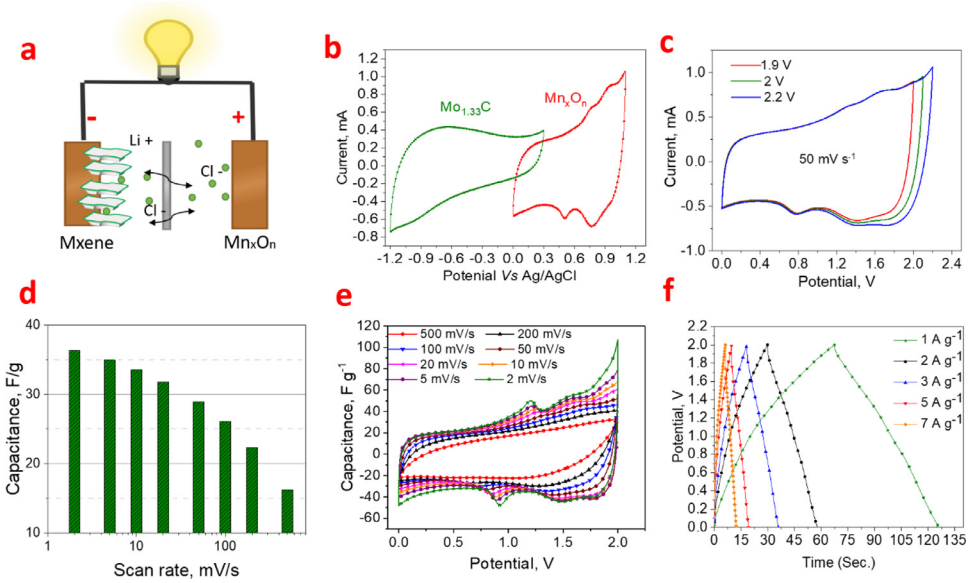

Fig. 3. The electrochemical performance of MXene//Mn_xO_n asymmetric supercapacitors: a) schematic illustration of the device design; b) CV curves of the positive and negative electrodes at 10 mV s^{-1}; c) CV curves of MXene//Mn_xO_n device at the scan rate of 50 mV s^{-1} in different voltage windows; (d) Gravimetric capacitance of MXene//Mn_xO_n device at different scan rates; e) CV curves of MXene//Mn_xO_n device at different scan rates (2-500 mV s^{-1}); and f) charge/discharge profiles of MXene//Mn_xO_n device at different current densities.

fered from low stability in aqueous electrolyte due to the high oxidation rate and restacking, retaining only ~30% of the initial capacitance after 1500 charge/discharge cycles in 5M LiCl electrolyte [17]. Furthermore, a Coulombic efficiency of almost 100% after 7000 charge/discharge cycles, as shown by GCD curves (inset in Fig. 2e), indicates that the $Mo_{1.33}C$ MXene electrode will deliver stable performance during further cycling. The partition analysis (Fig. S6) shows the capacitive contribution (grey pattern) *vs.* current at the scan rate of 5 mVs^{-1} and 50 mVs^{-1}. The gradual increase in capacitive contribution with the increase of scan rates is a typical feature of supercapacitive electrodes and indicates a rapid charge storage mechanism.

Prior to the fabrication of ASCs, the electrochemical behavior of the as-prepared Mn_xO_n in 5M LiCl electrolyte is assessed by carrying out three-electrode measurements. TheCV and GCPL curves of Mn_xO_n electrode in 5M LiCl aqueous electrolyte at different scan rates and current densities are shown in Fig. S7. The CV curve, recorded at 2 mVs^{-1}, exhibits two distinct pairs of reversible redox peaks (Fig. 2f), where the redox couples at 0.55/0.7 V and 0.81/0.88 V (*vs.* Ag/AgCl) correspond to redox reactions of MnO_4 and MnOOH, respectively [28]. Also, these redox peaks still appeared at higher scan rates (50 mVs^{-1}), indicating the occurrence of reversible pseudocapacitive charge storage mechanism and high-rate performance. Mn_xO_n electrode delivered a gravimetric capacitance of ~170 Fg^{-1} at the scan rate of 2 mVs^{1}.

TheASC is assembled using $Mo_{1.33}C$ MXene as negative electrode and Mn_xO_n as positive electrode, as schematically illustrated in Fig. 3a. The charge balance between both electrodes was achieved by adjusting the electrodes mass according to the charge storage capability in a specific potential window. The electrochemical behavior of the MXene and Mn_xO_n in a three-electrode configuration suggests that the voltage window can be extended to 2.4 V, as presented in Fig. 3b. Herein, the voltage window can be extended to 2.2 V without destroying the CV shape, as shown in Fig. 3c. However, the MXene//Mn_xO_n device exhibits stable performance in an operating voltage window of 2 V. We, therefore, select 2 V as our operating potential window. The MXene//Mn_xO_n device was pre-cycled in a voltage range of 2 V for 50 cycles, stabilizing the CV shape and completely saturating the electrode with 5M LiCl electrolyte, see Fig. S8. The CV curves of the MXene //Mn_xO_n device were recorded at different scan rates, ranging from 2 to 500 mVs^{-1}, showing semi-rectangular shape with prominent redox peaks, which belong to the change in oxidation states of Mn, as discussed earlier. The CV analysis confirms the pseudo-capacitive intercalation storage mechanism of the MXene//Mn_xO_n device. The gravimetric capacitance was calculated from the discharge area of the CV curves (Fig. 3e). The device capacitance was calculated based on the total mass of both electrodes, rendering a gravimetric capacitance of ~38 Fg^{-1} and 22 Fg^{-1} at the scan rate of 2 mVs^{-1} and 100 mVs^{-1}, respectively (Fig. 3d). Consistent with the CV curves, the GCPL curves at different current densities exhibited high symmetry, indicating excellent reversibility and Coulombic efficiency of the MXene-based ASCs (Fig. 3f).

As cyclic stability test is a crucial parameter to investigate the performance of ASCs, the charge/discharge stability was assessed at the current density of 10 Ag^{-1}. Fig. 4a shows that the $Mo_{1.33}C$//Mn_xO_n device exhibits an outstanding cyclic stability with the capacitance retention of 92% after 10,000 charge/discharge cycles. The superior cyclic stability can be attributed to the structural stability of $Mo_{1.33}C$ and Mn_xO_n during repeated charge and discharge processes. Additionally, the high reversibility of $Mo_{1.33}C$//Mn_xO_n device is confirmed as shown by the GCPL curves (inset in Fig. 4a), which confirms that the high Coulombic efficiency is achieved by avoiding the decomposition of aqueous electrolyte or other side reactions during the charge/discharge cycling. The performance of previously reported ASCs with binder-free MXene and MXene-based composite electrodes in LiCl electrolyte are exemplified through Ti_3C_2/30 wt.% Cheveral with retained 80% of the initial capacitance after only 1500 charge/discharge cycles [15], whereas a Ti_3C_2/Fe_2O_3 composite retained 79% of the initial capacitance after 5000 charge/discharge cycles in 5M LiCl [29]. Herein, the $Mo_{1.33}C$ //Mn_xO_n device retained 92% of the initial capacitance after 10,000 charge/discharge cycles, which shows the potential of $Mo_{1.33}C$ MXene in ASCs with LiCl electrolyte.

Both power and energy densities were calculated and plotted in the Ragone plot in Fig. 4b. The MXene//Mn_xO_n device exhibited an energy density of 19 Wh kg^{-1} (58 $mWhcm^{-3}$) and a power density of 1.08 W kg^{-1} (~ 3 Wcm^{-3}) at 1 Ag $^{-1}$. Maximum power density of 31 Wcm^{-3} was achieved at the current density of 10 A g^{-1}, corresponding to the energy density of ~32 $mWhcm^{-3}$. One should note that the volumetric energy density of the $Mo_{1\cdot33}C$//Mn_xO_n device is higher than all $Mo_{1\cdot33}C$ based devices irrespective of the type of the electrolyte,such as $Mo_{1\cdot33}C$//$Mo_{1.33}C$ and $Mo_{1.33}C$/PEDOT:PSS//$Mo_{1.33}C$/PEDOT:PSS symmetric devices in sulfuric acid [11]. Also, the volumetric energy density of the $Mo_{1\cdot33}C$//Mn_xO_n device combined with a high power density is higher than most MXenes based devices measured in different configurations, such as Ti_3C_2 porous//Ti_3C_2 porous, Ti_3C_2//graphene, Ti_3C_2//rGO, and V_2C//V_2C in aqueous electrolytes (only the highest values of the reports shown), as presented in the

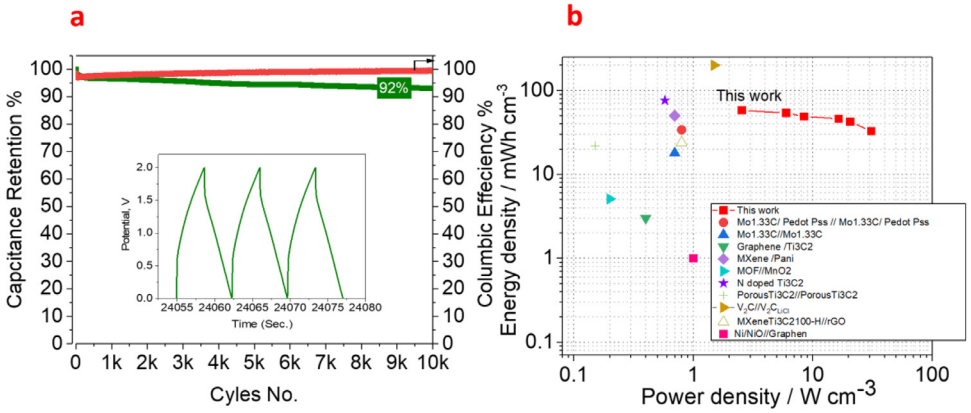

Fig. 4. (a) Capacitance retention and columbic efficiency of the ASC, where the inset shows the charge/discharge curves at the current density of 10 A g^{-1}; and b) The Ragone plot compares the energy and power densities of the $Mo_{1\cdot33}C//Mn_xO_n$ device with previously reported MXene-based devices in aqueous electrolytes.

Ragone plot [17,18,21,30-32]. Moreover, the achieved energy density is higher than asymmetric devices based on other 2D materials, such as Co_3O_4//graphene, Ni/NiO//graphene, and $TiO_2/MnO_2//TiO_2$ [33-35].

Conclusions

Despite the high charge storage capacitance, the $Mo_{1.33}C$ MXene based symmetric and asymmetric supercapacitors typically demonstrate moderate energy density due to the limited operating voltage window. Herein, the superior electrochemical performance of $Mo_{1.33}C$ MXene in LiCl electrolyte, i.e., high capacitance and large voltage window, is exploited to constructACS using Mn_xO_n as a positive electrode. Both binder-free $Mo_{1.33}C$ and Mn_xO_n electrodes exhibited a high capacitance of 217 Fg^{-1} and 170 Fg^{-1}, respectively, in three-electrode configurations at $2mVs^{-1}$. Owing to the high specific capacitance, good conductivity, rapid charge/discharge capability and high stability of both electrodes, $Mo_{1\cdot33}C//Mn_xO_n$ ASCs achieved a high volumetric energy density of 58 $mWhcm^{-3}$ and retained 92% of the initial capacitance after 10,000 charge/discharge cycles. The MXene//Mn_xO_n devices were operated in the voltage window of 2 V and GCD curves were recorded within long-term cycling, showing excellent Coulombic efficiency of 100%. These results support that high-capacitance electrodes, such as MXenes, should be investigated in different electrolytes and coupled with suitable positive electrodes to realize their full potential and utilization in practical applications.

Credit authorships

Ahmed EL Ghazaly: Conceptualization, Methodology, Investigation, Writing – original draft. **Wei Zheng:** Methodology, review & editing. **Joseph Halim**: MXene synthesis, review & editing. **Eric Tseng:** TEM analysis. **Per OA Persson**. TEM analysis, supervision**. Bilal Ahmed:** Writing – review & editing, Funding acquisition, and Co-supervision. **Johanna Rosen**: Methodology, Writing –review & editing, Funding acquisition, Supervision.

Declaration of Competing Interest

The authors declare no competing interests.

Acknowledgements

J.R. acknowledge support from the Knut and Alice Wallenberg (KAW) Foundation for a Fellowship/Scholar Grant and Project funding (KAW 2015.0043), and from the Swedish Foundation for Strategic Research (SSF) for Project Funding (EM16-0004). The KAW Foundation is also acknowledged for support to the Linköping Electron Microscopy Laboratory. Support from the Swedish Government Strategic Research Area in Materials Science on Functional Materials at Linköping University (Faculty Grant SFO-Mat-LiU No 2009 00971) is also acknowledged. B.A. acknowledges the support from Vinnova and the Swedish Strategy Group for EU-Coordination (2018-02677).

Supplementary materials

Supplementary material associated with this article can be found, in the online version, at doi:10.1016/j.ensm.2021.05.006.

References

[1] H. Tomiyasu, et al., An aqueous electrolyte of the widest potential window and its superior capability for capacitors, Sci. Rep. 7 (1) (2017) 45048.
[2] B. Pal, et al., Electrolyte selection for supercapacitive devices: a critical review, Nanoscale Adv. 1 (10) (2019) 3807–3835.
[3] M.R. Lukatskaya, et al., Ultra-high-rate pseudocapacitive energy storage in two-dimensional transition metal carbides, Nature Energy 2 (8) (2017) 17105.
[4] M. Ghidiu, et al., Conductive two-dimensional titanium carbide 'clay' with high volumetric capacitance, Nature 516 (7529) (2014) 78–81.
[5] M.R. Lukatskaya, et al., Cation Intercalation and High Volumetric Capacitance of Two-Dimensional Titanium Carbide, Science 341 (6153) (2013) 1502–1505.
[6] M. Naguib, et al., Two-Dimensional Nanocrystals Produced by Exfoliation of Ti3AlC2, Adv. Mater. 23 (37) (2011) 4248–4253.
[7] B. Ahmed, A.E. Ghazaly, J. Rosen, i-MXenes for Energy Storage and Catalysis, Adv. Funct. Mater. 30 (47) (2020) 2000894.
[8] Q. Tao, et al., Two-dimensional Mo1.33C MXene with divacancy ordering prepared from parent 3D laminate with in-plane chemical ordering, Nat. Commun. 8 (1) (2017) 14949.
[9] Hans Lind, et al., Investigation of vacancy-ordered M o 1.33 C MXene from first principles and x-ray photoelectron spectroscopy., Phys. Rev. Mater. 1 (4) (2017) 044002.
[10] A.S. Etman, J. Halim, J. Rosen, Fabrication of Mo1.33CTz (MXene)–cellulose freestanding electrodes for supercapacitor applications, Mater. Adv. 2 (2) (2021) 743–753.
[11] L. Qin, et al., High-Performance Ultrathin Flexible Solid-State Supercapacitors Based on Solution Processable Mo1.33C MXene and PEDOT:PSS, Adv. Funct. Mater. 28 (2) (2018) 1703808.
[12] L. Qin, et al., Flexible solid-state asymmetric supercapacitors with enhanced performance enabled by free-standing MXene–biopolymer nanocomposites and hierarchical graphene–RuOx paper electrodes, Batteries Supercaps 3 (7) (2020) 604–610.
[13] Y. Sun, et al., Proton Redox and Transport in MXene-Confined Water, ACS Appl. Mater. Interfaces 12 (1) (2020) 763–770.
[14] Y. Tian, et al., Understanding MXene-Based "Symmetric" Supercapacitors and Redox Electrolyte Energy Storage, ACS Appl. Energy Mater. 2020 3 (5) (2020) 5006–5014.
[15] F. Malchik, et al., Superfast high-energy storage hybrid device composed of MXene and Chevrel-phase electrodes operated in saturated LiCl electrolyte solution, J. Mater. Chem. A 7 (34) (2019) 19761–19773.
[16] I. Harsányi, L. Pusztai, Hydration structure in concentrated aqueous lithium chloride solutions: A reverse Monte Carlo based combination of molecular dynamics simulations and diffraction data, J. Chem. Phys. 137 (20) (2012) 204503.
[17] A. VahidMohammadi, et al., Assembling 2D MXenes into highly stable pseudocapacitive electrodes with high power and energy densities, Adv. Mater. 31 (8) (2019) 1806931.
[18] L. Yu, et al., MXene-bonded activated carbon as a flexible electrode for high-performance supercapacitors, ACS Energy Lett. 3 (7) (2018) 1597–1603.
[19] M. Boota, Y. Gogotsi, MXene—conducting polymer asymmetric pseudocapacitors, Adv. Energy Mater. 9 (7) (2019) 1802917.
[20] Q. Jiang, et al., All pseudocapacitive MXene-RuO2 asymmetric supercapacitors, Adv. Energy Mater. 8 (13) (2018) 1703043.

[21] T. Xiong, et al., Mn3O4/reduced graphene oxide based supercapacitor with ultra–long cycling performance, J. Mater. Chem. A 5 (25) (2017) 12762–12768.
[22] J.-K. Chang, et al., Physicochemical factors that affect the pseudocapacitance and cyclic stability of Mn oxide electrodes, Electrochim. Acta 54 (12) (2009) 3278–3284.
[23] R. Dong, et al., Enhanced Supercapacitor Performance of Mn3O4 Nanocrystals by Doping Transition-Metal Ions, ACS Appl. Mater. Interfaces 5 (19) (2013) 9508–9516.
[24] Y. Hu, et al., Controllable structure transitions of Mn3O4 nanomaterials and their effects on electrochemical properties, Nanoscale Horizons 2 (6) (2017) 326–332.
[25] J. Lu, et al., Sulfide cluster vacancies inducing an electrochemical reversibility improvement of titanium disulfide electrode material, J. Mater. Chem. A 8 (14) (2020) 6532–6538.
[26] H. Wu, et al., Vacancy-mediated lithium adsorption and diffusion on MXene, Appl. Surf. Sci. 488 (2019) 578–585.
[27] W. Zheng, et al., Boosting the volumetric capacitance of MoO3-x free-standing films with Ti3C2 MXene, Electrochim. Acta (2020) 137665.
[28] R. Chinnasamy, R.R. Thangavelu, Electrochemical behavior of β-MnO2 and MnOOH nanorods in different electrolytes, AIP Conf. Proc. 1665 (1) (2015) 050062.
[29] R. Zou, et al., Self-assembled MXene(Ti3C2Tx)/α-Fe2O3 nanocomposite as negative electrode material for supercapacitors, Electrochim. Acta 292 (2018) 31–38.
[30] L. Li, et al., Flexible Ti3C2Tx/PEDOT:PSS films with outstanding volumetric capacitance for asymmetric supercapacitors, Dalton Trans. 48 (5) (2019) 1747–1756.
[31] C. Yang, et al., Flexible Nitrogen-Doped 2D Titanium Carbides (MXene) Films Constructed by an Ex Situ Solvothermal Method with Extraordinary Volumetric Capacitance, Adv. Energy Mater. 8 (31) (2018) 1802087.
[32] L. Zhang, et al., A Review of Redox Electrolytes for Supercapacitors, Front. Chem. 8 (413) (2020).
[33] Y.-Z. Zhang, et al., Flexible Supercapacitors: A Simple Approach to Boost Capacitance: Flexible Supercapacitors Based on Manganese Oxides@MOFs via Chemically Induced In Situ Self-Transformation (Adv. Mater. 26/2016)., Adv. Mater. 28 (26) (2016) 5241–5241.
[34] A.N. Naveen, P. Manimaran, S. Selladurai, Cobalt oxide (Co3O4)/graphene nanosheets (GNS) composite prepared by novel route for supercapacitor application, J. Mater. Sci. Mater. Electron. 26 (11) (2015) 8988–9000.
[35] M. Yu, et al., Scalable self-growth of Ni@NiO core-shell electrode with ultrahigh capacitance and super-long cyclic stability for supercapacitors, NPG Asia Mater. 6 (9) (2014) e129–e129.